Course Project
AE 641
Navigation and Guidance

Group - 3

Ayush Bhaskar (23B0015)
Dawar Jyoti Deka (23B0036)

Course Instructor

Prof. Arnab Maity

Indian Institute of Technology Bombay

Problem 1 Solution

The system under consideration is a linear, time-invariant, discrete-time process described by the state evolution equation

$$x(k+1) = A\,x(k) + B\,w(k), \tag{1}$$

together with the scalar measurement model

$$y(k) = H\,x(k) + v(k). \tag{2}$$

The state vector

$$x(k) = \begin{bmatrix} x_1(k) \\ x_2(k) \end{bmatrix}$$

evolves according to the dynamics matrices

$$A = \begin{bmatrix} -\frac{1}{3} & 1 \\ \frac{1}{3} & 0 \end{bmatrix}, \qquad B = \begin{bmatrix} 0 \\ 1 \end{bmatrix},$$

while the sensor provides a single linear combination of the states through

$$H = \begin{bmatrix} 2 & 2 \end{bmatrix}.$$

Both process and measurement perturbations are modeled as independent, zero-mean, unit-variance Gaussian sequences,

$$w(k) \sim \mathcal{N}(0,1), \qquad v(k) \sim \mathcal{N}(0,1).$$

Since the process noise enters through B, the associated process covariance is

$$Q = BB^T = \begin{bmatrix} 0 & 0 \\ 0 & 1 \end{bmatrix},$$

and the measurement noise variance is

$$R = 1.$$

The initial conditions provided for the estimator are

$$\hat{x}(0|0) = \begin{bmatrix} 1 \\ 0 \end{bmatrix}, \qquad P(0|0) = I_2.$$

Under these assumptions, the optimal linear minimum-variance state estimator is the discrete Kalman filter. The time-propagated *a priori* estimates are obtained from

$$\hat{x}(k+1|k) = A\,\hat{x}(k|k), \tag{3}$$

$$P(k+1|k) = A\,P(k|k)\,A^T + Q, \tag{4}$$

capturing deterministic evolution and added uncertainty due to process noise.

Upon receiving the new measurement $y(k+1)$, the innovation is computed:

$$\tilde{y}(k+1) = y(k+1) - H\,\hat{x}(k+1|k), \tag{5}$$

with covariance

$$S(k+1) = H\,P(k+1|k)\,H^T + R. \tag{6}$$

The Kalman gain is then

$$K(k+1) = P(k+1|k)\,H^T\,S(k+1)^{-1}. \tag{7}$$

The updated state estimate and covariance are

$$\hat{x}(k+1|k+1) = \hat{x}(k+1|k) + K(k+1)\,\tilde{y}(k+1), \tag{8}$$

$$P(k+1|k+1) = (I - K(k+1)\,H)\,P(k+1|k). \tag{9}$$

These recursions fully describe the Kalman filtering process. Because the scalar measurement observes only the sum of the two states, reconstructibility requires sufficient coupling in the dynamics matrix A, which is satisfied here. The covariance evolution and Kalman gain reflect the anisotropic noise structure, since only the second state is directly influenced by stochastic excitation.

Summary of designed Kalman Filter

Prediction (Time Update)

$$\hat{x}_{k+1|k} = A\,\hat{x}_{k|k} = \begin{bmatrix} -\frac{1}{3} & 1 \\ \frac{1}{3} & 0 \end{bmatrix} \hat{x}_{k|k}$$

$$P_{k+1|k} = A\,P_{k|k}A^T + Q = A\,P_{k|k}A^T + \begin{bmatrix} 0 & 0 \\ 0 & 1 \end{bmatrix}$$

Update (Measurement Incorporation)

$$S = H\,P_{k+1|k}H^T + R = \begin{bmatrix} 2 & 2 \end{bmatrix} P_{k+1|k} \begin{bmatrix} 2 \\ 2 \end{bmatrix} + 1$$

$$K = P_{k+1|k}H^T S^{-1} = P_{k+1|k} \begin{bmatrix} 2 \\ 2 \end{bmatrix} S^{-1}$$

$$\hat{x}_{k+1|k+1} = \hat{x}_{k+1|k} + K\,(y_{k+1} - H\hat{x}_{k+1|k})$$

$$P_{k+1|k+1} = (I - KH)\,P_{k+1|k}$$

Matrix Values Recap

$$A = \begin{bmatrix} -\frac{1}{3} & 1 \\ \frac{1}{3} & 0 \end{bmatrix}, \qquad B = \begin{bmatrix} 0 \\ 1 \end{bmatrix}, \qquad H = \begin{bmatrix} 2 & 2 \end{bmatrix}$$

$$Q = BB^T = \begin{bmatrix} 0 & 0 \\ 0 & 1 \end{bmatrix}, \qquad R = 1$$

Assumptions, Kalman Filter Concept, and Source of True States

The system assumes zero-mean, white, Gaussian process noise

$$w(k) \sim \mathcal{N}(0, 1),$$

entering through the input matrix B, leading to the state-space process noise covariance

$$Q = BB^T = \begin{bmatrix} 0 & 0 \\ 0 & 1 \end{bmatrix}.$$

The measurement noise is modeled as

$$v(k) \sim \mathcal{N}(0, 1), \qquad R = 1.$$

The Kalman filter is initialized with the prior

$$\hat{x}(0|0) = \begin{bmatrix} 1 \\ 0 \end{bmatrix}, \qquad P(0|0) = I_2,$$

while the initial *true* state used for simulation is chosen as

$$x_{\text{true}}(0) = \begin{bmatrix} 0.5 \\ -0.2 \end{bmatrix},$$

solely for generating ground-truth trajectories. The process and measurement noises are assumed mutually independent and independent across time.

The Kalman Filter provides the minimum-variance linear estimate of the state by optimally combining the model-based prediction with noisy sensor observations. It outputs both an estimated state and an associated covariance, from which confidence intervals such as

$$\hat{x}(k|k) \;\pm\; 2\,\mathrm{diag}\big(P(k|k)\big)$$

are derived to quantify estimation uncertainty.

The "true state" used for comparison in simulation is generated directly from the state-space model

$$x_{\text{true}}(k+1) = A\,x_{\text{true}}(k) + B\,w(k),$$

and serves only as ground truth for evaluating the estimator. In real systems, the true state is never known, and only the filter estimates are available.

Simulation Plots: Short and Long Runs

Short-Run Trajectories

Short-Run Kalman Filter Results

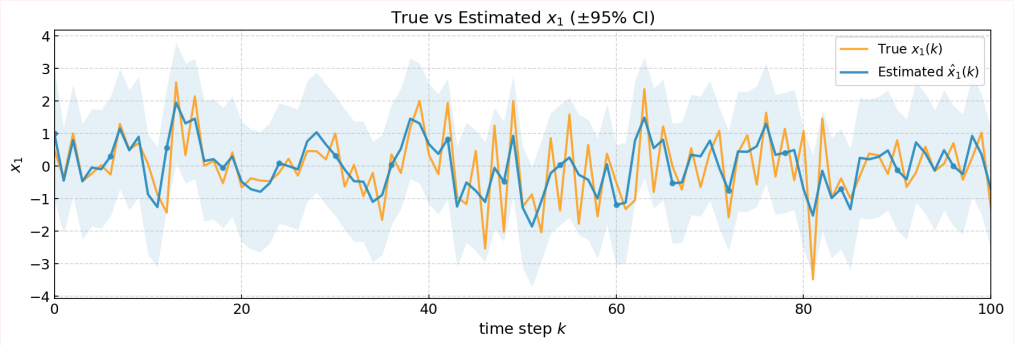

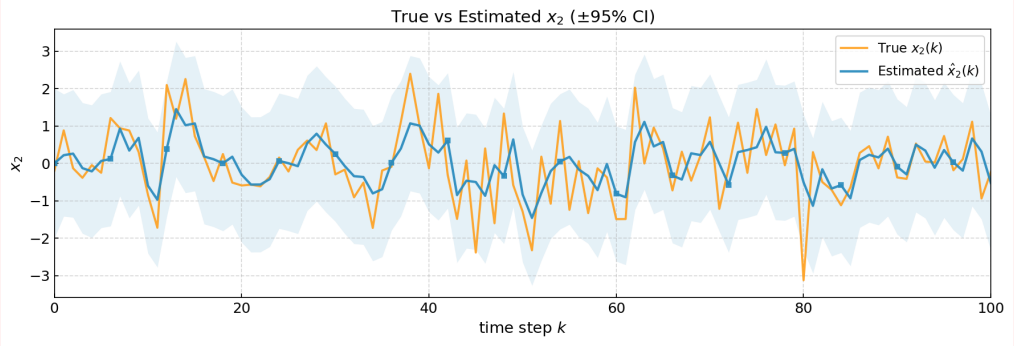

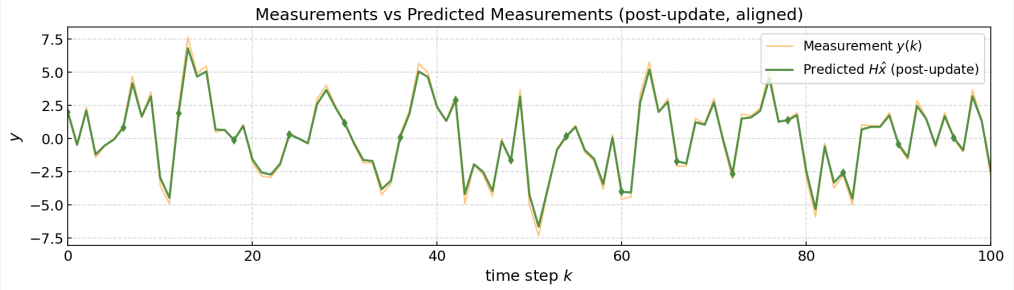

Observation and Discussion

The short-run results show that the Kalman Filter is able to track both state components accurately despite the presence of significant process and measurement noise. The estimated trajectories for $x_1(k)$ and $x_2(k)$ follow the corresponding true states closely, with only small deviations that remain largely within the predicted $\pm 2\sigma$ confidence bounds, demonstrating a well-behaved and consistent filter.

The measurement plot highlights the much higher variability of the raw sensor output compared to the smoother predicted measurement $H\hat{x}(k)$, reflecting the filter's ability to suppress noise and extract the underlying system dynamics.

Overall, the three plots confirm that the designed Kalman Filter performs correctly and reliably over the short horizon.

Long-Run Trajectories (Raw)

Long-Run Kalman Filter Results (Unprocessed)

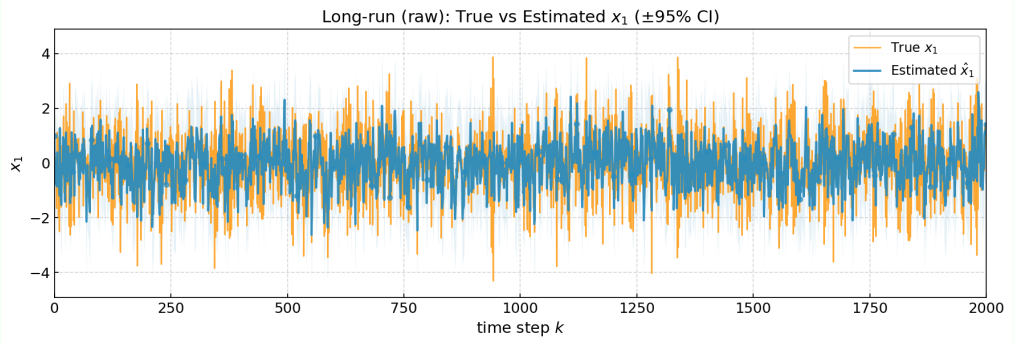

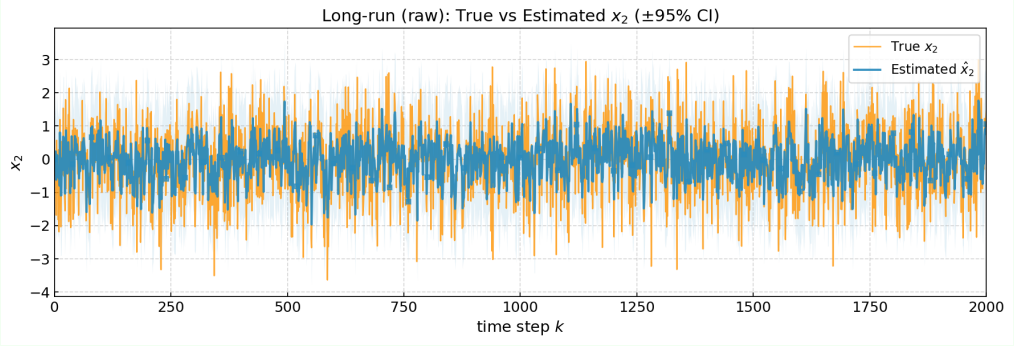

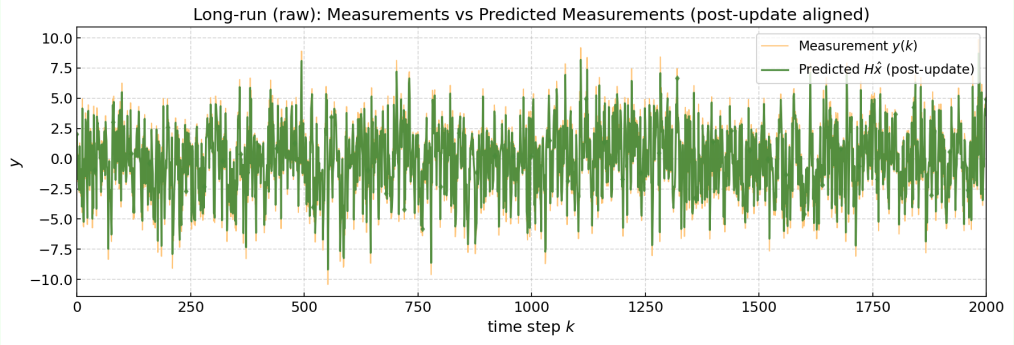

Observation and Discussion (Long Run -Raw)

Over the 2000-step horizon, the raw plots reflect the continuous influence of white process and measurement noise, producing highly fluctuating signals. Despite this, the Kalman Filter remains stable: the estimated states closely follow the true states, with both trajectories overlapping densely and the estimation error staying largely within the $\pm 2\sigma$ bounds.

The jagged appearance simply results from plotting every noisy sample, and this behaviour confirms that the filter maintains consistency and does not drift or diverge during long-term operation.

Long-Run Trajectories (Processed with Moving Average)

Long-Run Kalman Filter Results (Moving-Average Processed)

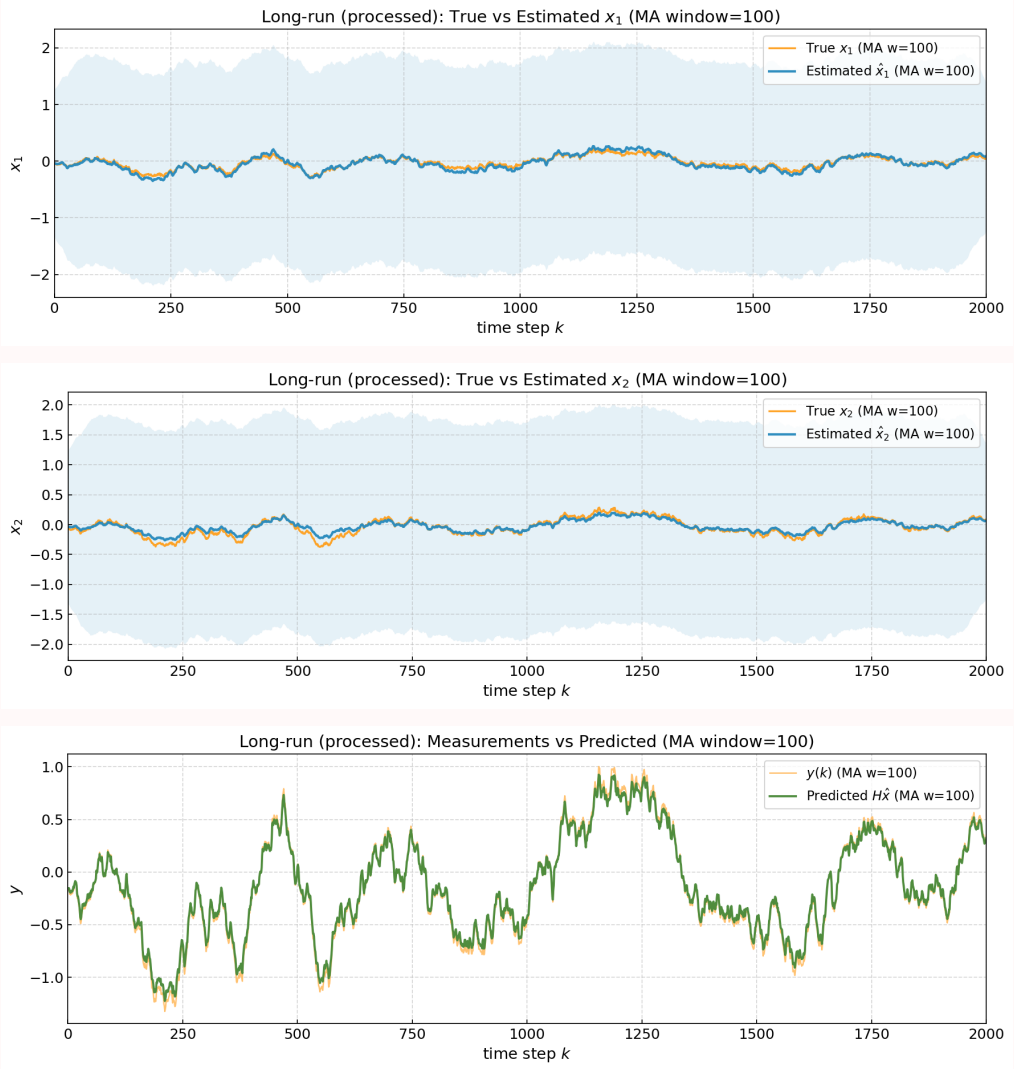

Observation and Discussion (Processed Long Runs)

With the moving-average smoothing applied, the long-run behaviour becomes much clearer: the noise is largely suppressed, exposing the slow underlying dynamics of the system. In this view, the Kalman Filter's estimates align almost perfectly with the true states throughout the 2000-step horizon, and the predicted measurements closely follow the smoothed observations.

Although the confidence bands widen over time, the filtered trajectories remain well centered, indicating stable and consistent long-term performance.

Final Kalman Filter Output

Final estimate $\hat{x}$:

$$\hat{x} = \begin{bmatrix} 1.40977087 \\ 1.05141781 \end{bmatrix}$$

Final covariance P:

$$P = \begin{bmatrix} 0.85251527 & -0.72453158 \\ -0.72453158 & 0.81630060 \end{bmatrix}$$

Moving-Average Post-Processing

The second set of figures (processed long-run plots) applies a moving-average FIR low-pass filter to each series. For a sequence $x[n]$ with window length W, the smoothed output is

$$x_{\mathrm{MA}}[n] = \frac{1}{W} \sum_{i=-\frac{W-1}{2}}^{\frac{W-1}{2}} x[n+i].$$

This is implemented using `np.convolve(..., mode='same')` with a normalized rectangular kernel (default $W = 100$). The `same` mode preserves the signal length, with boundary samples formed by partial kernel overlaps.

The moving average acts as a linear, time-invariant low-pass filter, reducing high-frequency noise while retaining slow dynamics. For visualization, the diagonal of $P_{k|k}$ is also smoothed before computing the $\pm 2\sigma$ bands, although the underlying Kalman Filter uses the unsmoothed covariance.

Problem statement 2

Consider an engagement scenario where the missile and target are launched from the ground and are initially separated by 50km. The target moves with constant speed V_T and constant flight–path angle α_T, while the missile moves with constant speed V_M under a deviated pursuit guidance law. The speed ratio is defined as

$$v = \frac{V_M}{V_T}.$$

In deviated pursuit, the missile velocity vector is directed at a constant deviation angle δ from the instantaneous line–of–sight (LOS) from missile to target.

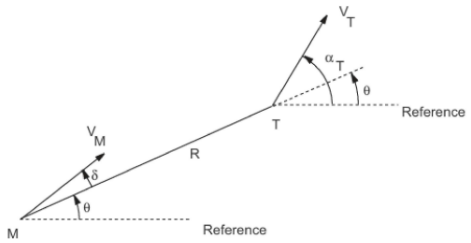

For a given set of parameters $(V_M, V_T, \alpha_T, \delta)$ specified in the project table, the tasks are:

- derive the planar engagement equations;
- obtain the missile and target trajectories in an inertial frame;
- compute the missile lateral acceleration history until interception;
- plot
  1. missile and target trajectories in inertial space, and
  2. time evolution of lateral acceleration of the missile,

  and comment on the lateral acceleration profiles for the given scenarios.

Coordinate frames and angles

The engagement is modeled in a two–dimensional horizontal plane. An inertial frame (O, X, Y) is defined with origin at the missile launch point, X horizontal and Y vertical (upwards). The target is launched from a point on the ground such that the initial range between missile and target is

$$R_0 = 50km.$$

At any time t:

- (x_M, y_M) and (x_T, y_T) denote missile and target inertial coordinates;
- R is the scalar range from missile to target;

- θ is the LOS angle, measured from the inertial X–axis to the line from missile to target;
- α_M and α_T are the missile and target flight–path angles relative to the X–axis.

The deviation angle δ for deviated pursuit is defined as the angular offset between the missile velocity direction and the LOS:

$$\delta = \alpha_M - \theta.$$

For conventional deviated pursuit, δ is held constant throughout the engagement.

Relative motion in polar form

Using the standard polar description with range R and LOS angle θ, the relative velocity between target and missile can be resolved along and normal to the LOS. The LOS–aligned component V_R and the transverse component V_θ are

$$V_R = \dot{R} = V_T \cos(\alpha_T - \theta) - V_M \cos\delta, \tag{10}$$

$$V_\theta = R\dot{\theta} = V_T \sin(\alpha_T - \theta) - V_M \sin\delta. \tag{11}$$

Equations (10)–(11) are the fundamental engagement equations for deviated pursuit with constant speeds and constant deviation angle.

These equations will be integrated numerically with appropriate initial conditions to obtain $R(t)$ and $\theta(t)$ until interception, defined by $R(t_f) \approx 0$ for some finite intercept time t_f.

Missile and target inertial trajectories

Target inertial motion

The target is assumed non–maneuvering, with constant speed V_T and constant flight–path angle α_T. Its inertial kinematics are

$$\dot{x}_T = V_T \cos\alpha_T, \tag{12}$$

$$\dot{y}_T = V_T \sin\alpha_T, \tag{13}$$

with initial position $(x_T(0), y_T(0))$ chosen such that the initial range between missile and target equals 50km. For example, if the missile is at the origin and the target initially lies on the X–axis,

$$x_T(0) = R_0 cos(\theta), \qquad y_T(0) = R_0 sin(\theta),$$

so that $R_0 = 50$ km

Missile inertial motion under deviated pursuit

The missile moves with constant speed V_M, but its flight–path angle α_M is determined by the deviated pursuit guidance law. Since δ is constant,

$$\alpha_M(t) = \theta(t) + \delta.$$

Hence the inertial kinematics of the missile are

$$\dot{x}_M = V_M \cos\alpha_M = V_M \cos(\theta + \delta), \tag{14}$$
$$\dot{y}_M = V_M \sin\alpha_M = V_M \sin(\theta + \delta). \tag{15}$$

At $t = 0$, the missile starts from the origin,

$$x_M(0) = 0, \qquad y_M(0) = 0.$$

The initial LOS angle is

$$\theta(0) = \tan^{-1}\left(\frac{y_T(0) - y_M(0)}{x_T(0) - x_M(0)}\right),$$

and the initial range is

$$R(0) = R_0 = \sqrt{(x_T(0) - x_M(0))^2 + (y_T(0) - y_M(0))^2}.$$

and thus range at any time t is:

$$R(t) = R_t = \sqrt{(x_T(t) - x_M(t))^2 + (y_T(t) - y_M(t))^2}.$$

Lateral acceleration of the missile

Definition

The missile lateral (normal) acceleration a_M is defined as the component of acceleration perpendicular to its velocity vector in the plane of motion. For constant speed motion in a plane, the magnitude of the normal acceleration is related to the flight–path angle rate:

$$a_M = V_M \dot{\alpha}_M.$$

Using the deviated pursuit relation $\alpha_M = \theta + \delta$ with constant δ, the missile flight–path angle rate is

$$\dot{\alpha}_M = \dot{\theta},$$

and therefore

$$a_M = V_M \dot{\theta}.$$

Expression in terms of relative motion

From (11),

$$R\dot{\theta} = V_T \sin(\alpha_T - \theta) - V_M \sin\delta,$$

hence

$$\dot{\theta} = \frac{V_T \sin(\alpha_T - \theta) - V_M \sin\delta}{R}.$$

Substituting into the expression for a_M gives

$$a_M = V_M \dot{\theta} = \frac{V_M}{R}\Big[\, V_T \sin(\alpha_T - \theta) - V_M \sin\delta \,\Big].$$

This relation shows explicitly how the instantaneous lateral acceleration depends on the current LOS angle θ, the range R, and the engagement parameters V_M, V_T and δ.

Non-dimensionalization and role of speed ratio

For analysis and comparison across scenarios, it is convenient to non–dimensionalize the equations using V_T and R_0. Define

$$\tau = \frac{V_T}{R_0} t, \qquad \rho = \frac{R}{R_0}.$$

Then the speed ratio $v = V_M/V_T$ appears explicitly in the scaled equations:

$$\frac{d\rho}{d\tau} = \cos(\alpha_T - \theta) - v\cos\delta, \tag{16}$$

$$\rho\frac{d\theta}{d\tau} = \sin(\alpha_T - \theta) - v\sin\delta. \tag{17}$$

The dimensionless lateral acceleration can be written as

$$\bar{a}_M = \frac{a_M R_0}{V_T^2} = K\,\rho^{-1}\Big[\sin(\alpha_T - \theta) - v\sin\delta\Big].$$

These forms highlight how larger K generally shortens intercept time but increases demanded lateral acceleration for a given δ.

Assumptions

The analysis is based on the following assumptions, consistent with the problem statement and standard deviated pursuit models:

- Planar engagement in a horizontal plane; out–of–plane motion is neglected.
- Gravity and aerodynamic drag are neglected in the guidance–level kinematics; V_M and V_T are constant.
- The target is non–maneuvering, with constant speed V_T and constant flight–path angle α_T.
- The missile can instantaneously generate any required lateral acceleration to maintain the deviated pursuit condition (no actuator or autopilot bandwidth limits).
- Seeker and sensor dynamics, measurement noise, and estimation errors are neglected; the LOS angle θ and its rate are assumed exactly known.
- Interception is declared when the range R falls below a small threshold (numerical tolerance).

These assumptions allow the focus to remain on the pure kinematic effects of deviated pursuit and the impact of (K, δ) on trajectories and acceleration demands.

Numerical solution procedure

The coupled first–order ODEs

$$\dot{R} = V_T \cos(\alpha_T - \theta) - V_M \cos\delta, \tag{18}$$

$$\dot{\theta} = \frac{V_T \sin(\alpha_T - \theta) - V_M \sin\delta}{R}, \tag{19}$$

$$\dot{x}_M = V_M \cos(\theta + \delta), \tag{20}$$

$$\dot{y}_M = V_M \sin(\theta + \delta), \tag{21}$$

$$\dot{x}_T = V_T \cos\alpha_T, \tag{22}$$

$$\dot{y}_T = V_T \sin\alpha_T, \tag{23}$$

are integrated numerically from $t = 0$ with specified initial conditions until interception. In `MATLAB` and `Python`), a fixed or adaptive time–step ODE solver(forward Euler method) is used.

At each time step, the missile lateral acceleration is computed from

$$a_M(t) = V_M \dot{\theta}(t),$$

with $\dot{\theta}(t)$ obtained either directly from the ODE or via the expression in terms of R and θ.

Results and discussion

For each engagement scenario in the project table (specified V_M, V_T, α_T, δ):

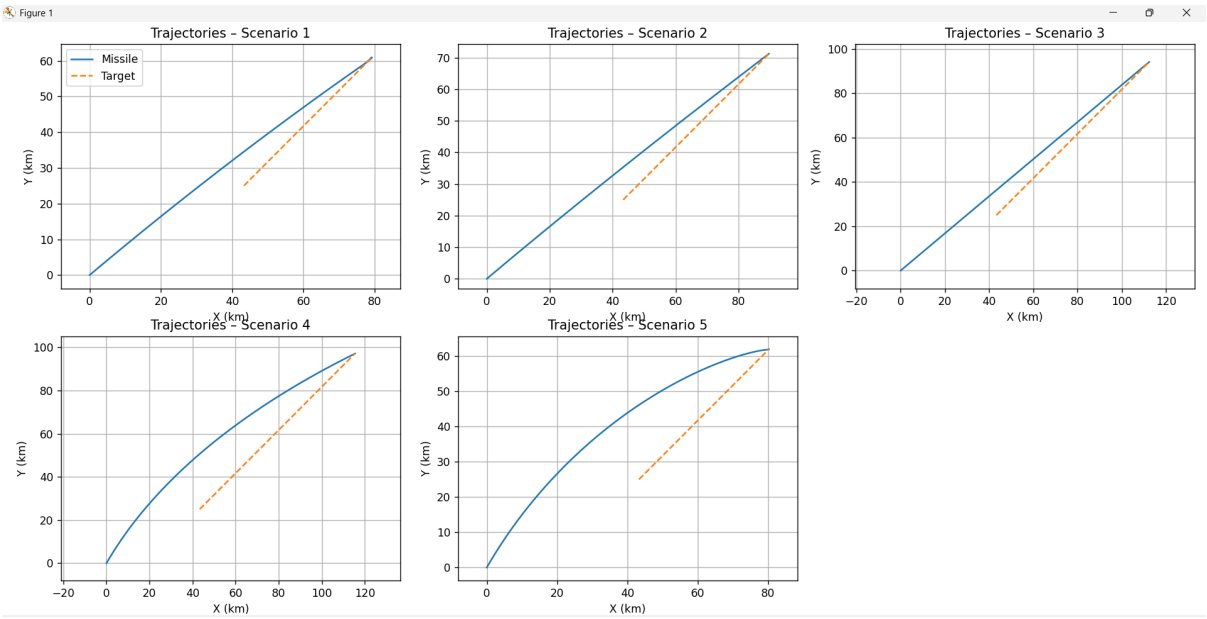

Figure 1: Trajectories plot for all scenarios

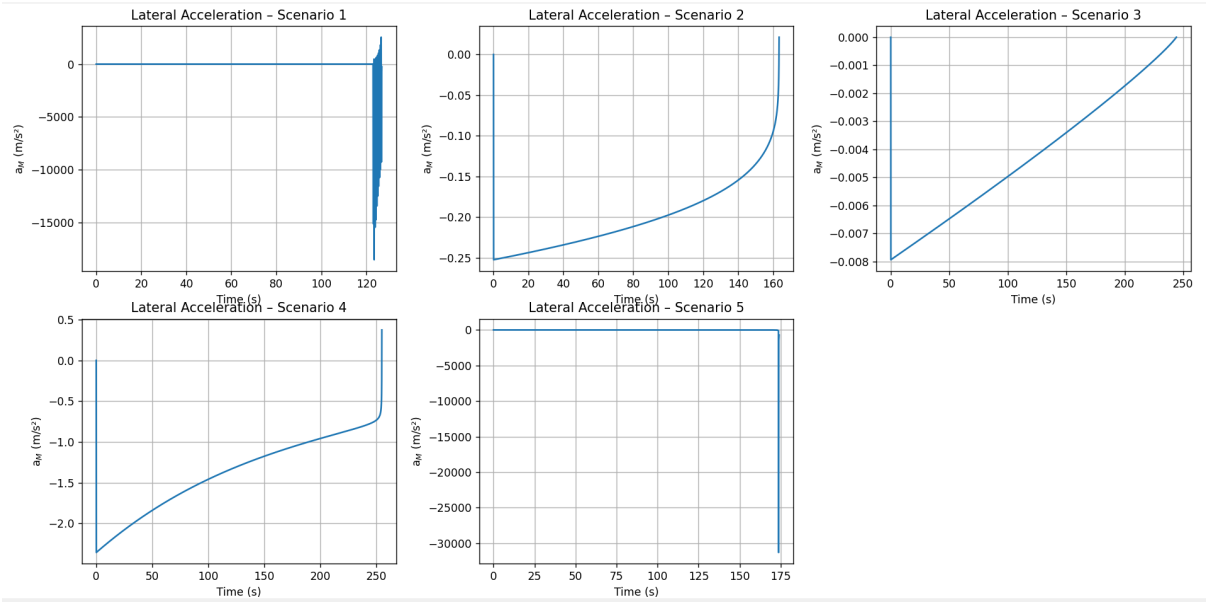

Figure 2: Plots for Lateral acceleration

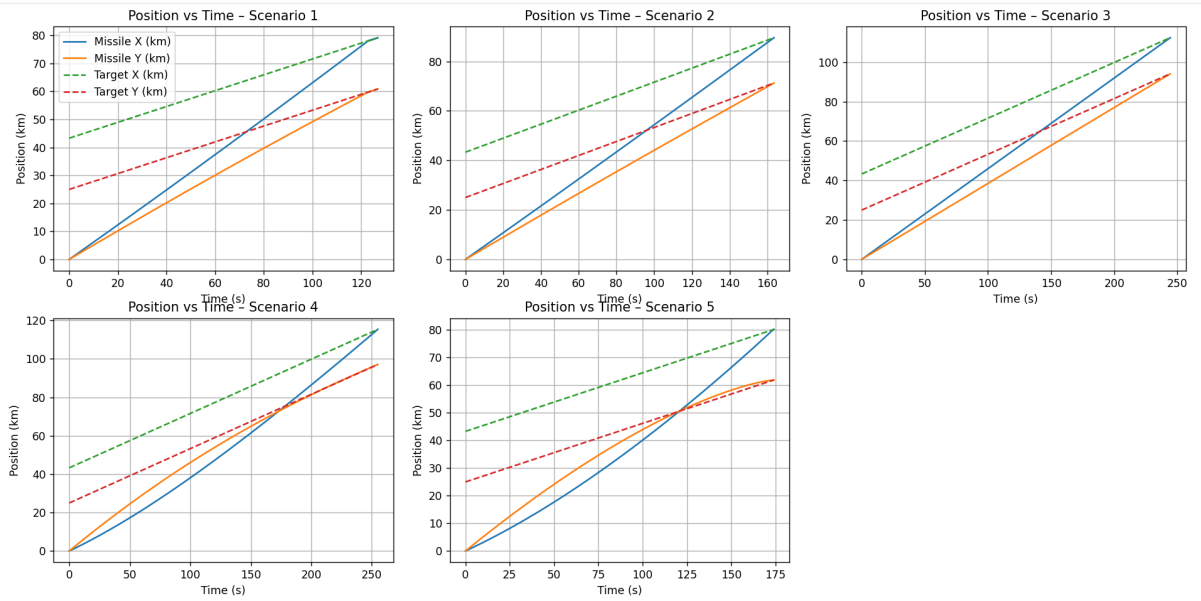

Figure 3: x and y coordinate plots with respect to time

Qualitative trends expected from deviated pursuit guidance are as follows:

- For small deviation angles δ, the missile path resembles pure pursuit, typically resulting in a curved trajectory that "lags" the target and may demand increasing lateral acceleration near interception.
- Increasing δ (up to an appropriate range) tends to straighten the missile trajectory and can reduce peak lateral acceleration, but also increases intercept time; very large δ can even prevent interception if the effective closing speed becomes too small.
- Larger speed ratios K reduce intercept time and allow successful interception for larger δ, but generally increase the magnitude of the required lateral acceleration for a given geometry.

In the report, these trends should be commented on with reference to the plotted trajectories and $a_M(t)$ profiles for the given scenarios.

Discussion of Lateral Acceleration Profiles

The lateral acceleration history $a_M(t)$ of the missile was obtained for all five engagement scenarios using the deviated pursuit engagement equations. In all cases, the qualitative shape of $a_M(t)$ is governed by the speed ratio

$$\nu = \frac{V_M}{V_T}$$

and the deviation angle δ, through the relation

$$R\dot{\theta} = V_T \sin(\alpha_T - \theta) - V_M \sin\delta, \qquad a_M = V_M\dot{\theta}.$$

As the engagement progresses and the range R decreases, the same numerator produces a larger $|\dot{\theta}|$ and hence a larger $|a_M|$, which explains the growth in acceleration magnitude as

interception is approached. Larger values of ν and/or larger δ typically lead to stronger lateral acceleration demand and more pronounced terminal build–up, in agreement with the theoretical condition $|\nu \sin \delta| < 1$ for a bounded deviated–pursuit solution.

Scenario 1 ($V_M = 800$ m/s, $V_T = 400$ m/s, $\delta = 10°$). For this relatively high speed ratio with a modest deviation angle, the lateral acceleration remains very small for most of the engagement, indicating a nearly straight flight path. As the missile closes in on the target and R becomes small, a_M exhibits a sharp spike with large negative values. This terminal blow–up is a consequence of the $1/R$ dependence in a_M and reflects the rapid change in line–of–sight angle just before the nominal collision point rather than a sustained high–g manoeuvre.

Scenario 2 ($V_M = 700$ m/s, $V_T = 400$ m/s, $\delta = 10°$). Reducing the missile speed while keeping the same deviation angle leads to a smoother and more moderate acceleration profile. The lateral acceleration starts with a small negative value and its magnitude gradually increases in time, but remains bounded throughout the engagement. The growth of $|a_M|$ near interception is visible but much less abrupt than in Scenario 1, indicating a more benign terminal manoeuvre.

Scenario 3 ($V_M = 600$ m/s, $V_T = 400$ m/s, $\delta = 10°$). With a further reduction in speed ratio, the required lateral acceleration is very low over the entire flight. The $a_M(t)$ curve shows a nearly linear variation from a small negative value towards zero, with no noticeable terminal spike. This case corresponds to a relatively gentle pursuit, with the missile requiring only mild continuous steering to maintain the collision course.

Scenario 4 ($V_M = 600$ m/s, $V_T = 400$ m/s, $\delta = 30°$). Here the speed ratio is the same as in Scenario 3, but the deviation angle is increased to 30°. The larger δ forces the missile to cut more aggressively inside the target path, which is reflected in a higher magnitude of lateral acceleration. The acceleration starts at a significantly larger negative value and its magnitude grows during most of the engagement, before turning slightly positive near interception. The profile remains bounded but clearly shows the stronger steering demand associated with a larger deviation angle.

Scenario 5 ($V_M = 600$ m/s, $V_T = 300$ m/s, $\delta = 30°$). This scenario combines a high speed ratio with a large deviation angle, giving $\nu \sin \delta \approx 1$, which lies on the theoretical boundary for the existence of a feasible deviated–pursuit solution. Numerically, the acceleration remains relatively small for a large portion of the flight, but as the missile approaches the target, R becomes very small and a_M exhibits a dramatic negative spike with extremely large magnitude. This unbounded growth is consistent with the theory: near the limit $|\nu \sin \delta| \to 1$, the line–of–sight rate and hence a_M become singular as the collision point is approached, indicating that such combinations of speed ratio and deviation angle are not practical from a guidance and control standpoint. In summary,

the simulated acceleration profiles confirm the expected trends: moderate ν and δ yield smooth and bounded $a_M(t)$, while aggressive combinations (high ν and/or large δ) lead to strong terminal acceleration build–up and, in the limiting case, to effectively unbounded lateral acceleration demands.

Conclusion

The deviated pursuit guidance law was numerically investigated for five engagement scenarios using both trajectory simulation and lateral–acceleration analysis. The study clearly demonstrated the fundamental differences between pure pursuit and deviated pursuit, and highlighted how the deviation angle δ influences the geometry and stability of the engagement.

For moderate deviation angles and reasonable speed ratios, deviated pursuit successfully guides the missile onto a collision course more efficiently than pure pursuit. This was observed in Scenarios 2, 3 and 4, where the trajectories converged smoothly and the lateral acceleration remained bounded and well within physically meaningful limits. These cases validate the engagement dynamics derived in the lecture notes, where the LOS rate $\dot{\theta}$ and missile acceleration $a_M = V_M\dot{\theta}$ evolve in a predictable manner.

In contrast, Scenarios 1 and 5 exhibited extremely large terminal accelerations as the missile approached interception. This behaviour is consistent with the theoretical conditions for the existence of a viable deviated–pursuit solution. Specifically, the boundedness requirement

$$|\nu \sin\delta| < 1, \qquad \nu = \frac{V_M}{V_T},$$

was violated in Scenario 5 and pushed to the limit in Scenario 1. As the range R becomes very small near collision, the term $a_M = V_M\dot{\theta}$ diverges, producing large spikes in lateral acceleration. These results do not represent numerical errors; rather, they reflect physical and geometric constraints intrinsic to the guidance law.

Overall, the project confirms that deviated pursuit can significantly improve interception geometry compared to pure pursuit, but only when the engagement parameters satisfy the theoretical feasibility conditions. Excessive deviation angles or large speed ratios can destabilize the pursuit, leading to unbounded LOS rates and unphysical accelerations. Thus, while deviated pursuit offers practical advantages in reducing path length and improving convergence, its applicability depends critically on selecting δ and ν within the stable operational region.